ON THE SPECIFIC TEMPORAL STRUCTURE OF RADIATION PULSES IN DENSE SCATTERING MEDIA. PART I. OBSERVATIONS OF THE SCATTERED RADIATION

V.V. Vergun, E.V. Genin, G.P. Kokhanenko, V.A. Krutikov, and D.S. Mezhevoi

Institute of Atmospheric Optics,
Siberian Branch of the Academy of Sciences of the USSR, Tomsk
Received February 13, 1990

The propagation of short laser pulses through dense fogs has been experimentally studied in an aerosol chamber. Instrumentation and processing techniques are described for measuring the scattered radiation and monitoring the optical parameters of the medium. Multiple scattering produces a depolarized background and its formation is studied. Temporal trends of the two depolarized components are compared with each other.

The study of the characteristics of laser pulse propagation through scattering media of large optical depths continues to attract the attention of many authors. Despite the successful development of techniques for solving the nonstationary radiation transfer problem,[1] and plentiful experimental data (e.g., in Refs. 2 and 3) the contradictory nature of the results presented by various authors still remains unexplained. Particularly poor is our present-day understanding of the polarization characteristics of transmitted radiation. The available theoretical results[4] principally refer to deep layers and to solar radiation, while experimental data[5] are hardly sufficient to explain the depolarization processes affecting radiation pulses as they penetrate into the depths of the scattering medium.

Therefore experiments conducted in model scattering media appear to be of particular importance (such media are generated in special aerosol chambers). These experiments make it possible to study under controlled conditions the dependence of pulse parameters on the geometric and optical propagation regime. At the same time the limited temporal resolution of the detectors used introduces distortions in the experimental results, particularly at low optical depths. Under such conditions combining physical experiments with numerical simulations becomes more effective.

This paper presents results from model experiments and Monte-Carlo simulations on the temporal structure and polarization properties of laser pulses in the beam axial zone, and investigates the effect of detector geometry upon the recorded pulse characteristics. The possibility of applying the diffusion approximation to describe the temporal structure of the pulses is discussed.

The first part of the paper is dedicated to a study of the shape of the polarized components in the signal. To carry out our model experiment in the large aerosol chamber (LAC) at the Institute of Atmospheric Optics, a special instrumentation setup was built. A block-diagram of it is presented in Fig. 1.

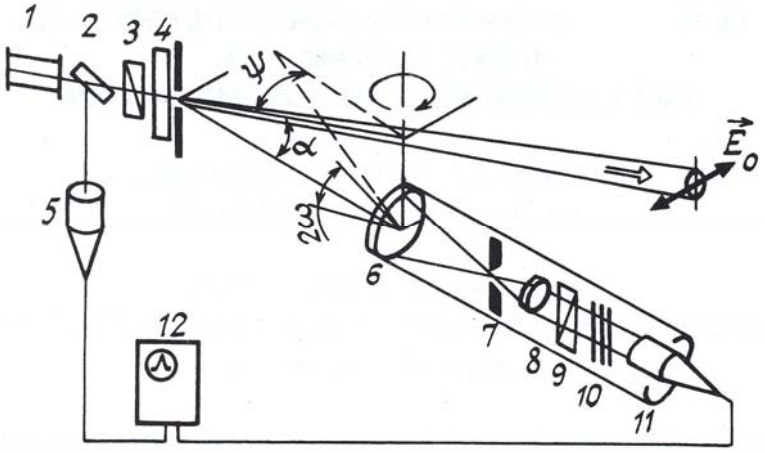

FIG. 1. Optical block-diagram of the experimental setup.

0235-6880/90/07 631-07 $02.00

A copper vapor optical quantum generator (OQG) was employed as the radiation source. The instrument was designed by the Scientific-Technical Complex at the Institute of Atmospheric Optics.[6] It operates in the self-heating regime, so as to provide a minimal pulse duration. Its operational characteristics are as follows: working wavelength — 510.6 nm, pulse repetition frequency — 5 kHz, pulse duration — (3–20) ns, pulse power — at least 10 kW, beam radius $2R_{source}$ = 10 mm, beam divergence ω_{source} = 10 min. The OQG 1 radiation passes through the splitting plate 2, the polaroid 3, and enters the chamber through the entrance window with diaphragm 4. The initial polarization of the beam is set so that the vector $\vec{E}_0$ is horizontal. The chamber totals 26 m in length and 10 m in diameter. The beam elevation above the chamber floor is 1.9 m. Twenty meters from the entrance window a polarization pulse photometer is positioned in the vertical plane containing the beam. Its polar angle α is set before the start of measurements by displacing the entire photometer in the vertical. During the measurements the azimuth angle ψ is varied by rotating the photometer in the horizontal within the limits 0–65°. . At $\psi = 0°$ the entrance window is within the photometer field of view. The photometer objective 6 (4.5/210 mm, R_{det} = 2.4 mm) and diaphragm 7 determine the detector field of view $\omega = 2°$. By rotating the polaroid 9 a component of the radiation is selected, polarized either parallel ($J_\parallel$) or perpendicular ($J_\perp$) to the initial polarization. The accuracy of selection of the polarization components from the signal is reduced by the capabilities of the polaroids used, and by possible parasitic scatterings of the optical surfaces. The chosen experimental scheme' (small scattering angle α, normal orientation of the initial polarization plane to the scattering plane) should have resulted in the absence of a cross-polarized component in the chamber at low experimental turbidities of the model medium ($\tau \ll 1$). Actual measurements taken in the chamber at such low turbidities and a scattering angle of $\alpha = 0.5°$ have demonstrated that the two-component signal ratio $J_\perp / J_\parallel$ is equal to $0.8–1.0 \cdot 10^{-3}$, and that azimuthal scanning within the limits $\psi = 0–2°$ does not change that ratio. The relationship $J_\perp = 10^{-3} J_\parallel$ thus represents the minimal detectable level for the cross-polarized component.

The set of light filters 10 consists of four neutral filters which can be introduced into the beam in any combination, so that the total extinction can vary from 1.3 to $4 \cdot 10^3$. Then the light pulse falls upon the photocathode of the fast photomultiplier (PM) 11 of the 18ÉLU-FM type. According to its specifications the temporal resolution of the PM is Δt = 2.1 ns at half the pulse amplitude at the PM anode. To record the signal a S7-13 two-channel stroboscopic oscilloscope 12 is used. The scanning is triggered by a baseline signal fed from the FK-2 coaxial photoelement (CP) 5. Since the OQG pulse shape and amplitude are quite stable, its stroboscopic recording significantly lowers the noise level by averaging over a large number of pulses (the recording time for one pulse varies within the range 8–20 s). The chosen triggering system guarantees reliable recording of the temporal delay of the scattered pulse with respect to its position at low chamber turbidities (i.e., in the case of single scattering only). Signals from the analog output of the stroboscopic oscilloscope are fed to ADC.

To produce adiabatic fogs in the chamber its pressure, which is first pumped to +1 atm, is dropped via a special vent with a regulated opening. The measurements were conducted under quite similar conditions of chamber venting (the maximum extinction coefficient was $\varepsilon = 4–2$ m^{-1}). After reaching its maximum density the fog starts to disperse, and the measured extinction coefficient uniformly decreases, so that the parameters of the scattered pulses were reproduced from realization to realization rather well. The fog dispersal time is about 20 minutes, so it was possible to measure the parameters of the scattered pulses at various azimuths, and, correspondingly, various path optical depths. The resulting dependences were obtained by averaging the measurements for various fog realizations.

The instruments needed to measure the optical parameters of the fog were placed within the LAC on the same level as the main radiation beam, somewhat off the path. The transparency sensor which served to monitor the medium extinction coefficient used radiation from an LG-38 OQG (λ = 0.63 μm). Depending on the fog density, the measurements were conducted at either of the two paths with baselines L_1 = 0.98 and L = 5 m. Signals from the narrow angle sensors ($\omega = 3'$) were averaged over the complete record. Fog inhomogeneities result in errors in the measurements of the optical depth measurement which, when reduced to a 20 m path length, are equivalent to $\tau = \pm 1$.

In the case of not too thick fogs ($\varepsilon < 0.5$ m^{-1}) their scattering phase function was measured by a small angle photometer positioned 20 meters from the entrance window. It operated within the angles 0.8–30° angles using the "slipping volume" technique. To measure the same phase function in denser fogs within the 3–10° angle range an aureole photometer was used. It measured the angular distribution of the OQG radiation in the objective focal plane, after the beam had passed through a fog layer 0.5 m thick.

Analysis of the measured scattering phase function[7] demonstrates that the optical properties of stationary adiabatic fogs (i.e., those with extinction coefficient decreasing within the range $\varepsilon = 4–0.5$ m^{-1}) are close to the Deirmenjian Cl cloud model. Hence our model layer experiments appear applicable for studying the propagation of laser pulses through actual clouds and fogs.

All the LAC windows are equipped with diaphragms to exclude glint .from the glass, and the

chamber walls are painted opaque black to reduce parasitic scatterings. In addition all the optical elements are heated (including the LAC windows and the photometer objectives) so that they will not mist while the chamber is being pumped up.

The automated system of data recording and processing, based on a SM-1420 "Elektronika-60" computer, records the signals coming from the pulse photometer and the CP, and continuously records the optical parameters of the medium, i.e., the extinction coefficient and the scattering phase function within the angles 20′–3°. It also rotates the optical table following a special program to obtain the angular scan (to the accuracy of the rotation angle reading of 2′), controls the setting of the light filters and the polarizer, as well as the sensitivity of the measuring instruments. This automated system provides the possibility of further application of diverse mathematical processing techniques to large sets of experimental data.

The final experimental output includes the retrieved pulse transmission functions (PTF) which characterize the medium response to a $\delta(t)$-pulse. The signal recorded by the optical detector $U(t)$ is equal to the convolution of the PTF $J(t)$ and the instrument function $K(t)$

$$\int_0^t K(t-\tau)\, J(\tau)\, d\tau = U(t). \qquad (1)$$

In its turn, the function $K(t)$ is given by the convolution of the initial pulse $J_0(t)$ and the temporal response of the PM to a $\delta(t)$-pulse. The effect of the instrument function is particularly strong for model measurements in smaller aerosol chambers, since the distension of the temporal pulse then becomes comparable with the duration of the initial pulse. Retrieving the PTF from the solution of Eq. (1) and transforming to dimensionless parameters, we can then correctly extend our experimental results to environmental optical paths.

The solution techniques which make use of various regularization algorithms are quite well developed for equations of the type (1). We, in particular, employed the regularization algorithm described in Ref. 8, which applies, a discrete Fourier transform to the finite difference approximation of the Tikhonov functional, and is programmed as a fast Fourier transform. The experimentally recorded pulse scattered by a medium of low optical depth $\tau \ll 1$ was used for the equation kernel $K(t)$. Such a technique is capable of automatically accounting for the temporal resolution of the PM and for signal distortions in the recording tract. The pulses were further processed by the ADC at 128 points, at a discretization step of 0.5 ns. The PTF was then retrieved, with a regularization parameter selected for such an operation from a quasioptimal criterion. Physical considerations forced us to discard from the series those retrieved points in the PTF which appeared to have negative intensities as well as those with $t < 0$. The estimated error in the duration of the PTF did not exceed 1 ns at the 0.5 amplitude level.

Examples of pulse temporal profiles for the polarized components as recorded during our experiments at various optical depths are given in Refs. 6 and, 9. Figures 2 and 3 show the PTF of the medium, retrieved with the initial pulse shape taken into account. These results were obtained for $\alpha = 1.8°$ and $\psi = 0°$. The polarized components of the signal in Fig. 2 are given in normalized form for various optical depths. Pulse distension becomes noticeable starting from $\tau = 7$ for $J_\parallel$ and from $\tau = 12$ for $J_\perp$, the maximum lag — from $\tau = 20$ (for $J_\parallel$) and $\tau = 16$ (for $J_\perp$). Figure 3 compares the polarized components for identical optical depths (the dashed line shows the cross-polarized component). It is seen that the pulse front retains its polarization down to large optical depths, so that even at $\tau = 55$ a complete signal, depolarization is reached only after the pulse maximum passes the observation point. Since the amplitude ratio $J_\parallel / J_\perp$ is equal to 200 at $\tau = 19$, the scale has been changed for the $J_\perp$ component in the figure. It can be seen that even at small depolarizations pulse blooming and a delay in its maximum are noticeable in the cross-polarized component.

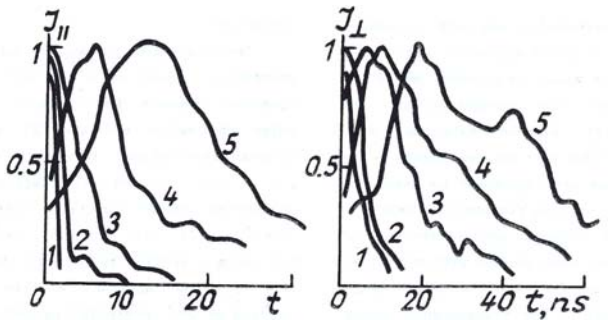

FIG. 2. Variations in the polarization component shapes for large layer optical depths. For $J_\parallel$: τ = 7 (1), 20 (2), 25 (3), 35 (4), 42 (5). For $J_\perp$: τ = 12 (1), 16 (2), 22 (3), 37 (4), 57 (5).

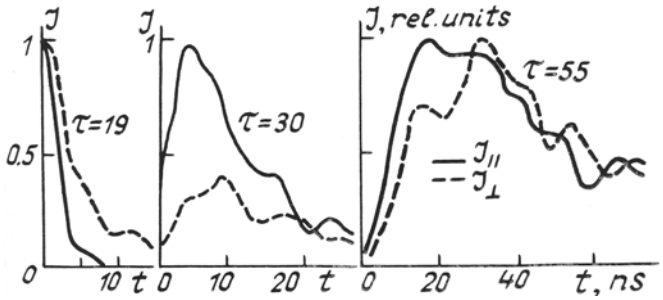

FIG. 3. Shapes of the pulse polarization components

In an isotropic scattering medium a cross-polarized component in the axial beam region is generated at large optical depths as a result of radiation depolarization due to multiple scattering. Taking that fact into account, we define the degree of depolarization as the ratio of the depolarized component to the total radiation flux: $\delta = 1 - P = 1 - (J_\parallel - J_\perp) / (J_\parallel + J_\perp)$. An analysis of the pulse depolarization (Fig. 4) shows that for any τ it depends uniquely on the dimensionless quantity $u = \varepsilon ct$, which has the meaning of the average scattering multiplicity for photons arriving at the detector at the moment t.

For $u > 25$ the pulse is practically completely depolarized (the value of $u = 25$ corresponds, at $\tau = 71$, to the pulse maximum). At $\tau > 30$ the pulse shape can be described by an approximate expression of the form

$$J(t) = ct^m \exp\left(-mt/t_{max}\right), \qquad (2)$$

if t is the time that has passed since the moment of pulse arrival in a weakly turbid medium. The ratio of pulse duration to the delay of its maximum ($\Delta t / t_{max}$) is approximately the same for all the pulses in the $J_\parallel$ component, and amounts to 2.6 ($m = 1$ in Eq. (2)). Such a delay of the maximum is longer for the depolarized component, $\Delta t / t_{max} \approx 2$, which corresponds to $m = 1.5$ in Eq. (2).

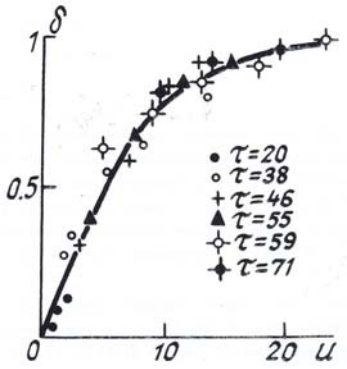

FIG. 4. Depolarization vs dimensionless time for photons arriving from various optical depths.

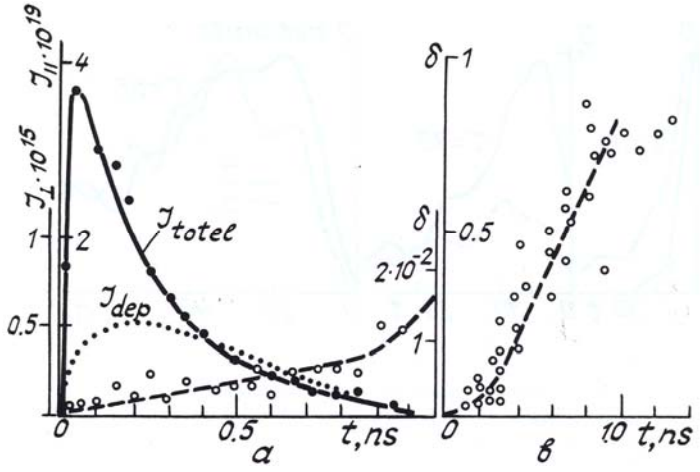

FIG. 5. Computed polarized components and pulse depolarization.

For the layer optical depth $\tau = 10$ experimental data on depolarization remain within the measurement error (at the level of $\delta < 10^{-3}$). Numerical simulations were conducted for that case using the local estimate algorithms[10] capable of computing the Stokes vector of the transmitted radiation for arbitrary position of both the source and the detector. The geometry of the calculation coincides completely with the experimental scheme, and we employed the elements of the scattering matrix computed for a water droplet aerosol

in Ref. 11 as the optical parameters of the medium. The calculational results for observation angles of $\alpha = 1.8^\circ$ and $\psi = 40^\circ$ are given in Fig. 5. The depolarized component is slightly extended and the depolarization itself (as given by the expression $\delta = 1 - P = 1 - \sqrt{S_1^2 + S_2^2 + S_3^2} / S_0$, where S_1 are the Stokes parameters for the scattered radiation) grows monotonically for longer photon arrival times, but remains insignificant within the main part of the pulse, i.e., down to 0.1 of its amplitude ($\delta < 10^{-2}$). This depolarization becomes large only at distant fall off of the pulse. The calculated rate of depolarization is twice as large as that observed in the experiment (Fig. 4) in the direction of the source.

Experiments and numerical estimate of the pulse shape deep within the scattering medium described in this paper demonstrate that the multiply scattered depolarized background produces a certain temporal structure of the pulse, such that the optical signal blooms and depolarizes as a result.

REFERENCES

1. E.P. Zege, A.P. Ivanov, and I.L. Katsev, *Image Transfer in Scattering Media* (Nauka i Tekhnika, Minsk, 1986).
2. V.K. Gavrikov and V.G. Korenev, Izv. Akad. Nauk SSSR, Ser. FAO **17**, No. 7, 763 (1981).
3. R.A. Eliott, Appl. Opt. **22**, No. 17, 2670 (1983).
4. E.P. Zege and L.I. Chaikovskaya, Izv. Akad. Nauk SSSR, Ser. FAO **17**, No. 8, 820 (1981).
5. Yu.A. Gol'din and V.N. Pelevin, *Hydrophysical and Optical Studies in the Indian Ocean* (Nauka, Moscow, 1975).
6. V.V. Vergun, A.E. Kirillov, G.P. Kokhanenko, V.L. Kruglyakov, and V.A. Krutikov, *"Application of a copper-vapor OQG to oservations of temporal distortions of scattered radiation,"* Dep. No. 2568-B86, February 27, 1986.
7. V.V. Vergun, M.V. Kabanov, G.P. Kokhanenko, V.A. Krutikov, M.V. Panchenko, and V.V. Pol'kin, Izv. Akad. Nauk SSSR, Ser. FAO **22**, No. 4, 403 (1988).
8. A.N. Tikhonov, A.V. Goncharskiĭ, et al., *Regularizing Algorithms and A-Priori Information* (Nauka, Moscow, 1983), 200 pp.
9. V.V. Vergun, M.V. Kabanov, G.P. Kokhanenko, and V.A. Krutikov, Opt. Atm. **1**, No. 2, 99 (1988).
10. G.I. Marchuk et al., *The Monte Carlo Methods in Atmospheric Optics* (Springer, Berlin, 1980).
11. V.E. Zuev, G.M. Krekov, G.G Matvienko, and A.I. Popkov, *Laser Sensing of the Atmosphere* (Nauka, Moscow, 1976), pp. 29–46.